Sub Topic: Soot

SAND2019-2863C

11th U. S. National Combustion Meeting
Organized by the Western States Section of the Combustion Institute
March 24–27, 2019
Pasadena, California

Soot Concentration, Temperature, and Radiant Emission Measurements in a Turbulent Ethylene Jet Flame

Christopher R. Shaddix, Jiayao Zhang, and Timothy C. Williams*

Combustion Research Facility, Sandia National Laboratories, Livermore, CA 94550 USA
**Corresponding Author Email: crshadd@sandia.gov*

Abstract: This work reports on a combined set of measurements of soot concentration, soot temperature, and radiant emission in a turbulent ethylene non-premixed jet flame with a jet exit Reynolds number of 20,000. The soot concentration measurements were measured via trapping-corrected laser-induced incandescence (LII) and validated via full-flame extinction. Soot temperature was measured simultaneously with soot concentration via an extinction/emission diagnostic with a local probe volume determined by two thin refractory probes. Radiant emission was quantified with a custom-built narrow-angle radiometer. The soot concentrations peak at a mean value of 0.6 ppm at mid-height of this flame. Mean soot temperatures are in the vicinity of 1550 K through the middle of the flame and then drop off near the top of the flame. Higher mean soot temperatures are found over the lower portion of the flame, reaching 1600 K along the centerline and 1730 K in the annulus. Evaluation of simultaneous OH PLIF/soot LII images taken in this flame explains these trends in soot temperature. The mean radiant emission peaks at 17.5 kW/m^2-sr, at nearly the same height as the peak of the mean soot volume fraction. This combined set of carefully measured and analyzed data from a burner designed for comparison with modeling results is a useful target for numerical predictions of turbulent sooty flames with a significant soot concentration.

Keywords: soot, radiation, temperature, flame

1. Introduction

The health effects of fine particulate matter (PM2.5) in ambient air have become increasingly evident over the past two decades. These particles deeply penetrate lung tissue and have been shown to affect the pulmonary and cardiovascular systems, leading to increased morbidity and mortality [1]. There have been many studies attempting to differentiate health effects from different components of PM2.5, with mixed success. It is clear, however, that soot particles (elemental carbon) contribute to the health impacts of PM2.5 [2-4]. Because of this association between soot particles in the atmosphere and deleterious health, soot emissions from combustion sources have faced increasingly stringent regulation. Furthermore, atmospheric soot has been shown to enhance climate forcing [5], and in-flight emission of soot from aircraft engines has been shown to influence contrail/cloud formation [6].

Despite decades of efforts, the R&D community still lacks a truly predictive modeling capability for soot formation and emission in turbulent flames, as characterize internal combustion engines, gas turbines, and furnaces. Soot formation has resisted efforts to develop effective models because of the complexity of the chemical reactions that are involved and their relatively long temporal duration, making soot formation very sensitive to local flame strain and differential diffusion, and their temporal dynamics. Beyond the complexity of the phenomena themselves,

another reason for the lack of predictive models is the lack of robust, spatially and temporally resolved data in sooting turbulent flames. Such datasets have been in development for many years for soot-free flames [7] and more recently for a slightly sooting methane flame [8], but available experimental datasets for moderate sooting turbulent flames are largely lacking. Such datasets are needed because under moderately sooting flame conditions, the soot that is formed radiates energy away from the hottest soot-containing regions to the walls of enclosures and to the cooler soot-containing regions of the flame, thus redistributing the reaction enthalpy and influencing the flame chemistry and burning rate in a coupled manner [9]. The ability of computational models to accurately describe these coupled soot formation/radiation/flame chemistry interactions cannot be tested with data from soot-free or lightly sooting flames.

Previously, we have reported on the design of piloted, turbulent jet flame burners for using higher hydrocarbon fuels, specifically on two designs for studying ethylene flames and flames fueled by prevaporized aviation fuel [10]. We also showed results for soot laser-induced incandescence (LII) and OH planar laser-induced fluorescence (PLIF) imaging in canonical ethylene and JP-8 surrogate jet flames with a fuel exit Reynolds number of 20,000 [11-12], as well as radiant emission profiles from these flames [13] and preliminary results for the joint soot temperature-volume fraction statistics, as determined with a '3-line' laser-optical diagnostic approach [14].

In this paper we present the full set of analyzed soot temperature data and integrate this new information with the previously reported soot concentration and radiant emission data for the ethylene turbulent flame, to give a complete set of measurements.

2. Experimental Methods

Measurements were performed in a piloted turbulent non-premixed ethylene jet flame stabilized on a burner designed along the same principle as the well-known Sydney burner [15]. The burner has a central fuel tube with a 3.35 mm ID and a concentric outer tube with a 19.1 mm OD. A pilot plate is situated in the annulus between the two tubes, recessed from the lip, and contains three concentric rows of equally distributed holes, supporting tiny flames for stabilizing the primary jet flame. While the central jet was composed of pure ethylene, a premixed ethylene/air mixture at an equivalence ratio of 0.9 was supplied to the pilot holes at a flow rate corresponding to 2% of the energy release rate of the main jet. With this design, the jet flames showed good flame attachment, even for fuel jet Reynolds numbers (Re) exceeding 30,000. The burner was positioned on top of a vertical wind tunnel that provided co-flowing dry air at 0.6 m/s, to prevent room-air disturbance and provide well-established boundary conditions for flame modeling. The whole assembly was mounted on a platform with XYZ translation to easily change the flame measurement location.

A flame with a fuel jet Reynolds number of 20,000 (corresponding to a fuel mass flow rate of 26.4 slpm at 298 K) was investigated in this study. This flame has sufficiently strong turbulence to minimize the influence of buoyancy and to test the robustness of combustion models but avoids frequent local flame extinction events in the high-shear region just above the burner lip (as verified with OH PLIF imaging [10]). Jet flames with flame extinction and subsequent reignition pose a major challenge for flame modeling [16], even in the absence of soot and its associated radiant heat transfer. For the broadest applicability to near-term turbulent flame modeling, it seemed prudent to perform measurements in a flame without significant local

extinction. The heat release rate of the flame was 24.0 kW and it had a visible flame height of approximately 870 mm.

To keep the paper length reasonable, only an overview of the various diagnostic methods that were employed is provided here. Our previous papers have described these methods in detail.

Soot concentration was determined using LII, as excited by the fundamental infrared (IR) output of a Nd:YAG laser (1064 nm) that was expanded into a sheet and trimmed to a height of 47 mm. The thickness of the laser sheet, defined as the $1/e^2$ width, was found to be 275 μm, with a variation of less than 15% across the field-of-view of the imaging camera. A laser pulse energy of 66 mJ was used, giving a fluence of 0.6 J/cm^2. The LII fluence response was found to give a nominally flat 'plateau' from 0.3 to 0.7 J/cm^2. Therefore, the LII signal was nearly independent of shot-to-shot fluctuations in the laser power or attenuation of the laser sheet as it passed through the sooty flame. The LII signals were collected by a Princeton Instruments intensified, fast-gating CCD camera mounted perpendicular to the laser path. The camera had a full-frame 512×512 CCD array and was set to image an area of 60×60 mm^2 (117 μm on each pixel). It was equipped with a Nikkor 50-mm focal length f/1.2 lens (Nikon), and the LII signal was collected through a Schott BG-14 glass filter and a 600-nm short-pass filter, effectively accepting light from 300 to 600 nm. The camera gate was set to 50 ns with zero delay from the laser pulse. The LII signals were calibrated for soot volume fraction by performing both LII imaging and laser extinction measurements with a cw HeNe laser (632.8 nm) on a laminar ethylene jet flame with a cold flow velocity of 0.41 m/s, anchored on the same jet burner as used for the turbulent flame. The transmitted laser light was collected in an integrating sphere and then detected on a photodiode after passing through a laser line filter. The soot concentration was deduced from the measured extinction using a dimensionless extinction coefficient, K_e, of 9.3, which is an average of those determined for soot sampled from laminar ethylene diffusion flames by Williams et al. [17] and which also corresponds to a midpoint value of the range of dimensionless extinction coefficients reported for soot emitted from both laminar and turbulent ethylene flames [17].

Radiant emission from the flame was measured with a custom-built radiometer that consisted of a thin-film thermopile detector (Dexter, Type 1M), with a calcium fluoride window that transmits radiation between 0.2 – 8 μm, which covers nearly all of the important radiation from flames. A black-anodized, water-cooled steel tube that is attached to the radiometer restricts incident radiation to a small solid angle (Ω) of 1.065 x 10^{-4} sr. The detector sensor was located 500 mm away from the jet axis. During experiments, the burner was traversed axially or radially to measure radiation along different paths. As the radiative heat exchange and the electronic response of the thermopile detector are affected by its own temperature, care was taken to stabilize the thermal environment of the detector. The radiometer signals were calibrated using a high-temperature blackbody source as a reference.

Joint soot temperature/concentration measurements were performed using a '3-line' simultaneous measurement of HeNe laser extinction and two-color emission from an optical sampling volume within the flame, as determined from the space separating two uncooled, alumina refractory probes (see Fig. 1). The probes had an OD of 0.25 in. (6.35 mm) and an ID of 0.175 in. (4.45 mm). A small flow of nitrogen (< 1 slpm) was introduced into each probe end to keep soot from flowing into the tubes. The two probe ends were separated by 10 mm, thereby defining the effective spatial resolution of the measurement. After passing through the flame probe volume, the laser beam was separated from the 2-color soot emission signals with the use of a dichroic beamsplitter. The transmitted beam was collected in a 12-inch (30.5-cm) diameter

integrating sphere, before passing through a laser line filter onto a photodiode detector, to remove any influence from turbulent flame beam steering on the attenuation measurement. Calibration of the two-color pyrometry diagnostic was performed using a high-temperature blackbody source with a mirror that redirected the blackbody light to the avalanche photodiode detectors.

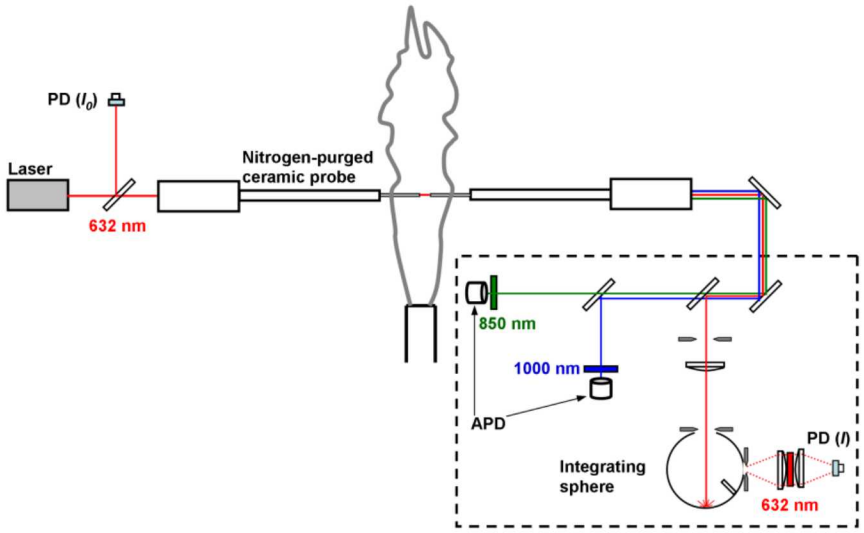

Figure 1. Schematic of diagnostic configuration used to perform 3-line measurements of soot temperature/concentration statistics in the turbulent jet flame.

3. Results and Discussion

Figure 2 shows the signal-trapping corrected time-averaged soot volume fraction radial profiles through the ethylene flame, after the profiles have been symmetrized (as required for the signal trapping correction). For the trapping correction, a dimensionless absorption coefficient K_a of 7.4 was used, as supported both by Bond and Bergstrom [18] for black carbon in the atmosphere and by the measurements of Williams et al. [17]. The full-flame centerline extinction measured with a HeNe laser is shown in Fig. 3. This measurement is useful not only in determining self-consistency in the quantification of the LII data [12] but also in giving a qualitative comparison to the radiant emission data, which also has a full-flame, line-of-sight characteristic.

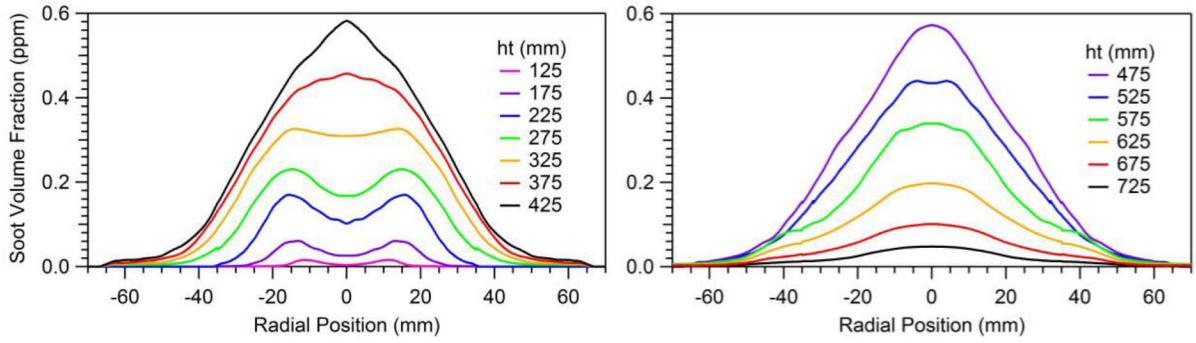

Figure 2. Signal-trapping corrected, time-averaged soot volume fraction profiles in the ethylene jet flame. The flame heights listed correspond to steps of 15 units when expressed as z/d, starting at z/d = 37.

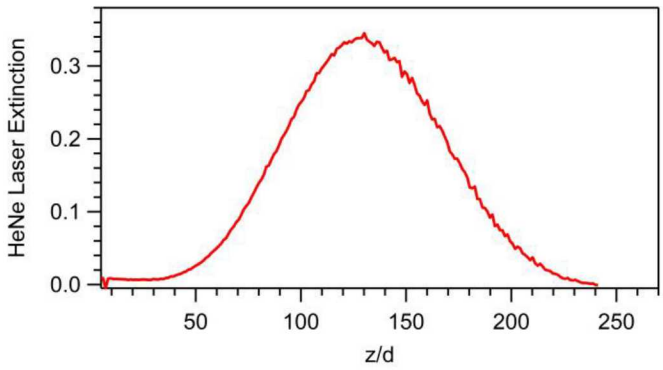

Figure 3. Time-averaged full-flame HeNe extinction along the jet axis centerline, as a function of the height above burner normalized by the burner diameter (z/d).

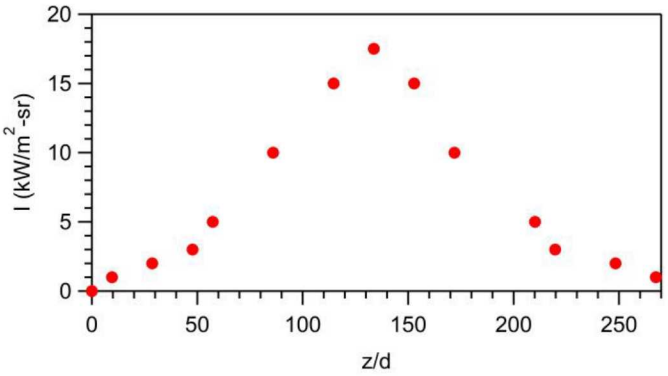

Figure 4. Time-averaged radiant emission along the jet axis centerline, as a function of the height above burner normalized by the burner diameter (z/d).

The centerline radiant emission is shown in Fig. 4. It is clear from comparing Figs. 3 and 4 that the soot optical thickness (as represented by the full-flame HeNe laser extinction) shows the same general profile as the radiant emission from the flame, suggesting a strong contribution of radiation from soot to the overall flame emission.

Figure 5 shows the time-averaged soot temperature profiles measured along the centerline of the flame, together with the standard deviation in temperature. At those points (at high and low extremes) where the standard deviation exceeded 200 K, the data was judged to be too uncertain to have confidence in it and is not shown in the figure. The centerline temperature profile appears to have an unusual shape, since it starts high, decreases quickly, then hits a plateau before rising again as the oxidation zone is approached, and then ultimately decreases through the oxidation zone. The most surprising aspect of this profile is the highest soot temperatures low in the flame, but it is important to recall that this measurement of soot temperature only makes a measurement at those instants when soot is present within the optical probe volume and the only contribution to the measured signal arises from those regions of the probe volume that contain soot at that moment in time. Therefore, it cannot be equated to a general measurement (or modeling prediction) of gas temperature at a given location.

In fact, an examination of the OH PLIF/LII imaging that was performed in this flame gives insight into the physics that explains the soot temperature profile shown in Fig. 5. As shown in Fig. 6, low down in the flame, soot begins to form near the OH layer on the edge of the flame.

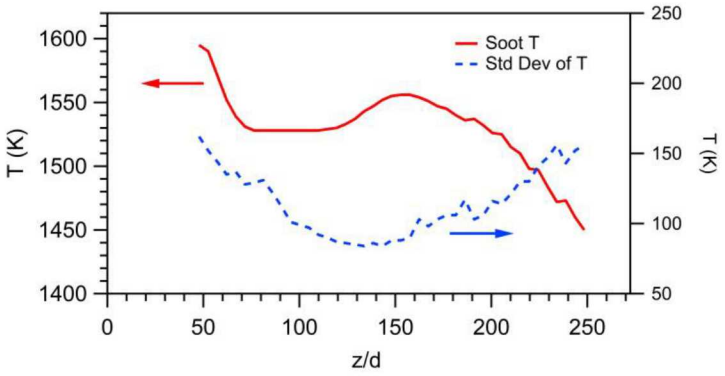

Figure 5. Time-averaged soot temperatures and standard deviation in soot temperature, as measured along the jet axis centerline, as a function of the height above burner normalized by the burner diameter (z/d).

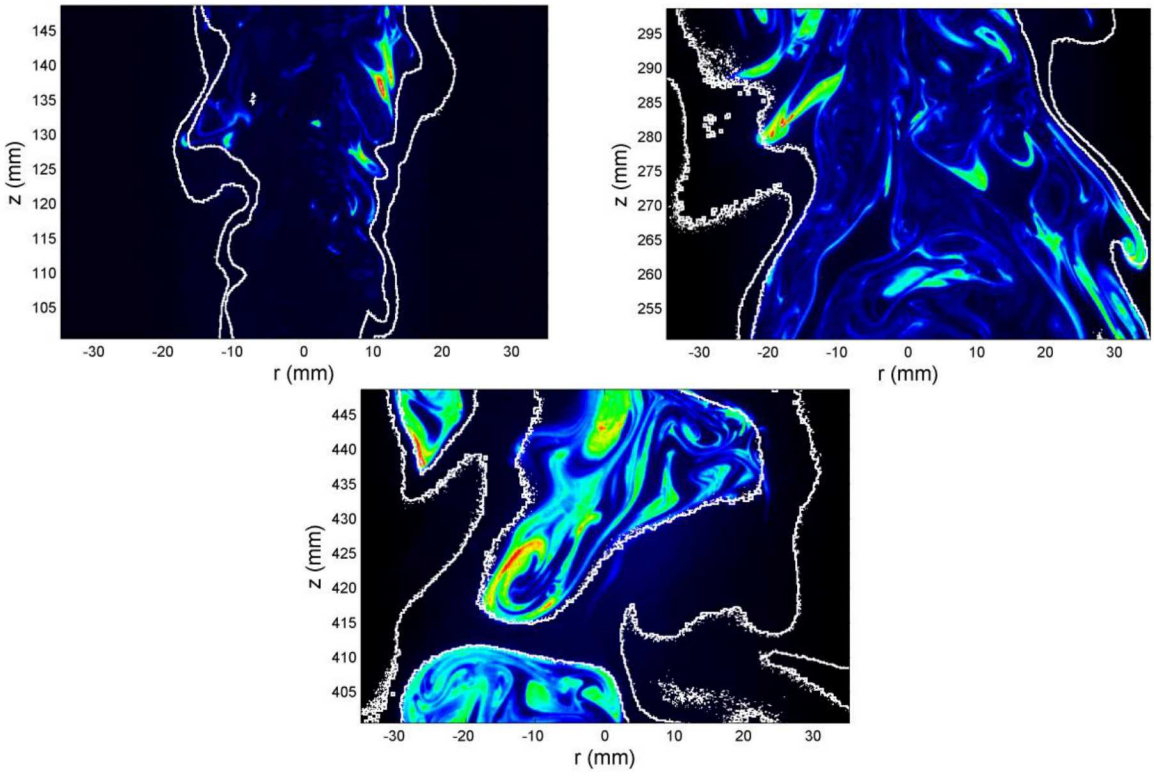

Figure 6. Overlay images of OH layer outlines (in white) on top of simultaneous LII images of soot concentration in the ethylene flame, at three different heights. For comparison of these images with the data in the previous plots, the top left image spans a z/d from 30-44, the top right image spans z/d from 75-89, and the bottom image spans z/d from 119-134.

The flame has not entrained much air at these lower positions, so the soot is limited to a narrow range of radial positions, as seen in the LII data in Fig. 2. During those times that soot does make it to the centerline at these lower positions, it is due to an occasional strong interior vortex that pulls soot over from the flame front region and/or an occasional strong vortex outside the flame sheet that drives it inward. In either case, the soot on the centerline is fairly hot. As one moves up the flame, the flame itself widens and the concerted action of the turbulence within the fuel jet mixes the soot that had formed near the flame front throughout the fuel-rich core of the jet. This mixing action cools the soot and also gives the soot time to radiate energy away and cool in this manner. As most of the fuel becomes consumed, the flame front moves inward in large vortical motions that allow the OH layer to reach the centerline and to clip-off soot-filled regions of the remaining fuel pyrolysis products. Initially this action leads to additional heating of the soot, due to its closer proximity to the flame front. However, radiant emission from the soot ultimately takes its toll and cools the gases, leading to a decreasing soot temperature as it is ultimately consumed.

The measured radial profiles of soot temperature support this interpretive description from the OH PLIF/LII images. Fig. 7 shows a few selected radial profile measurements. Clearly the highest time-average soot temperatures occur low in the flame, shortly after soot has begun to form, and show a strong annular character. Further up, the soot temperature profiles flatten and then ultimately decrease through the oxidation zone. Fig. 8 gives a more complete selection of the measurements, staggered to give an overall impression of the spatial trends in the data.

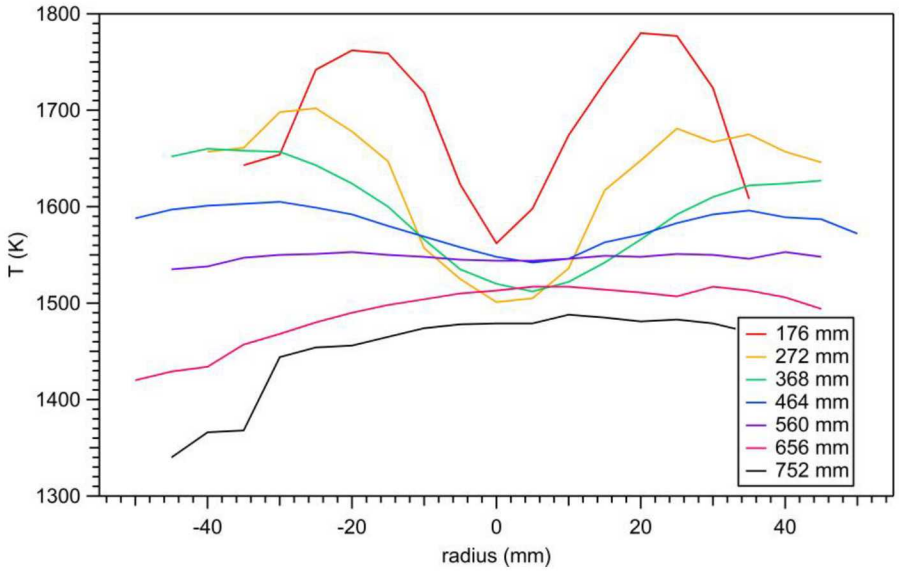

Figure 7. Radial profiles of time-averaged soot temperature at select heights from the bottom to top of the region of the flame with good quality temperature data.

The contribution of soot radiation to the overall radiant emission from the flame is determined by the full joint pdf of soot concentration and soot temperature throughout the flame. This information, which is also available from the 3-color measurements, is currently undergoing analysis.

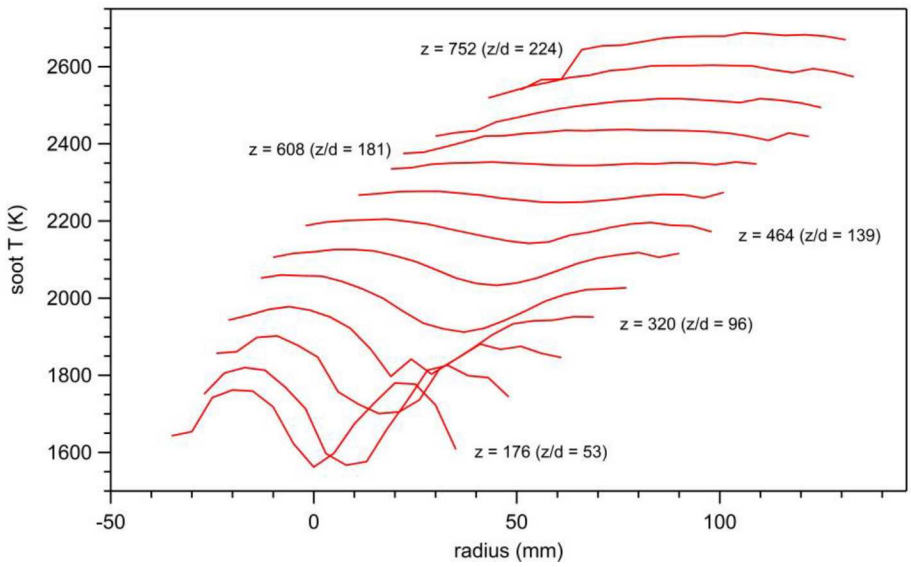

Figure 8. Staggered radial profiles of soot temperature. Each profile is staggered from the next lower in height by 100 K in temperature and 8 mm in radial position.

4. Conclusions

We have been reporting measurement results from a fairly strongly turbulent (Re = 20,000) non-premixed ethylene jet flame with well-defined boundary conditions for several years. In this paper we present the full set of analyzed time-averaged soot temperature data and integrate this new information with the previously reported soot concentration and radiant emission data. The time-averaged temperatures give perhaps a surprising trend of soot temperature peaking low in the flame, but an evaluation of previously collected simultaneous OH PLIF and soot LII images explains the flame physics behind the trends in the soot temperature data. This integrated set of measurements should comprise a challenging target for comparisons with turbulent flame models that include soot formation and radiant transport.

5. Acknowledgements

This work was supported by the U.S. DoD's Strategic Environmental Research and Development Program (SERDP). Sandia National Laboratories is a multimission laboratory managed and operated by National Technology and Engineering Solutions of Sandia, LLC., a wholly owned subsidiary of Honeywell International, Inc., for the U.S. Department of Energy's National Nuclear Security Administration under contract DE-NA-0003525. The views expressed in the article do not necessarily represent the views of the U.S. Department of Energy or the United States Government.

6. References

[1] R.D. Brook, S. Rajagopalan, C.A. Pope, J.R. Brook, A. Bhatnagar, A.V. Diez-Roux, F. Holguin, Y.L. Hong, R.V. Luepker, M.A. Mittleman, A. Peters, D. Siscovick, S.C. Smith, L. Whitsel, J.D. Kaufman Circulation 121 (2010) 2331-2378.

[2] A.C. Rohr, R.E. Wyzga, Atmos. Envir. 62 (2012) 130-152.

[3] A. Rohr, J. McDonald, Crit. Rev. Toxic. 46 (2016) 97-137.

[4] J. Yang, P. Roth, C.R. Ruehl, M.M. Shafer, D.S. Antkiewicz, T.D. Durbin, D. Cocker, A. Asa-Awuka, G. Karavalakis, Sci. Total Envir. 650 (2019) 1182-1194.

[5] R. Wang, Y. Balkanski, O. Boucher, P. Ciais, G.L. Schuster, F. Chevallier, B.H. Samset, J. Liu, S. Piao, M. Valari, S. Tao, J. Geophys. Res. Atmos. 121 (2015) 5948-5971.

[6] R. Watson, J. Houghton, D. Yihui, B. Metz, O. Davidson, N. Sundararaman, D. Griggs, D. Dokken, *Aviation and the Global Atmosphere*, a special report of the Intergovernmental Panel on Climate Change (IPCC), 1999, available from http://www.ipcc.ch/ipccreports/sres/aviation/index.htm

[7] R.S. Barlow, Proc. Combust. Instit. 31 (2007) 49-75.

[8] N.H. Qamar, Z.T. Alwahabi, Q.N. Chan, G.J. Nathan, D. Roekaerts, K.D. King, Combust. Flame 156 (2009) 1339-1347.

[9] A. Gupta, D.C. Haworth, M.F. Modest, Proc. Combust. Instit. 34 (2013) 1281-1288.

[10] J. Zhang, C.R. Shaddix, R.W. Schefer, Rev. Sci. Instr.82 (2011) 074101.

[11] J. Zhang, C.R. Shaddix, R.W. Schefer, Proceedings of the Western States Section of the Combustion Institute, Paper 09F-57, Oct. 26-27, 2009, UC Irvine, Irvine, CA.

[12] C.R. Shaddix, J. Zhang, T.C. Williams, Proceedings of the Western States Section of the Combustion Institute, Paper 2B-07, Mar. 21-22, 2016, University of Washington, Seattle, WA.

[13] C.R. Shaddix, J. Zhang, Proceedings of the Western States Section of the Combustion Institute, Paper 14S-07, Mar. 24-25, 2014, CalTech, Pasadena, CA.

[14] C.R. Shaddix, J. Zhang, Proceedings of the 8th US National Combustion Meeting, Paper 070LT-0100, May 19-22, 2013, Park City, UT.

[15] A.R. Masri, R.W. Dibble, R.S. Barlow Prog. Energy Combust. Sci. 22 (1996) 307-362.

[16] K. Gkagkas, R.P. Lindstedt, T.S. Kuan, Flow Turb. Combust. 82 (2009) 493-509.

[17] T.C. Williams, C.R. Shaddix, K.A. Jensen, J.M. Suo-Anttila, Int. J. Heat Mass Trans. 50 (2007) 1616-1630.

[18] T.C. Bond, R.H. Bergstrom, Aerosol Sci. Tech. 40 (2006) 27-67.